Published in final edited form as:
*Mol Cancer Ther*. 2012 June ; 11(6): 1365–1372. doi:10.1158/1535-7163.MCT-11-0764.

# Effect of Small Molecule Binding Affinity on Tumor Uptake *In Vivo*: A Systematic Study Using a Pretargeted Bispecific Antibody

**Kelly Davis Orcutt**[1], **John J Rhoden**[1], **Benjamin Ruiz-Yi**[1], **John V Frangioni**[4,5], and **K Dane Wittrup**[1,2,3]

[1]Department of Chemical Engineering, Massachusetts Institute of Technology, Cambridge, MA 02139

[2]Department of Biological Engineering, Massachusetts Institute of Technology, Cambridge, MA 02139

[3]Koch Institute for Integrative Cancer Research, Massachusetts Institute of Technology, Cambridge, MA 02139

[4]Department of Medicine, Beth Israel Deaconess Medical Center, Boston, MA 02215

[5]Department of Radiology, Beth Israel Deaconess Medical Center, Boston, MA 02215

## Abstract

Small molecule ligands specific for tumor-associated surface receptors have wide applications in cancer diagnosis and therapy. Achieving high-affinity binding to the desired target is important for improving detection limits and for increasing therapeutic efficacy. However, the affinity required for maximal binding and retention remains unknown. Here, we present a systematic study of the effect of small molecule affinity on tumor uptake *in vivo* with affinities spanning a range of three orders of magnitude. A pretargeted bispecific antibody with different binding affinities to different DOTA-based small molecules is used as a receptor proxy. In this particular system targeting carcinoembryonic antigen, a small-molecule binding affinity of 400 pM was sufficient to achieve maximal tumor targeting, and an improvement in affinity to 10 pM showed no significant improvement in tumor uptake at 24 h post-injection. We derive a simple mathematical model of tumor targeting using measurable parameters that correlates well with experimental observations. We use relations derived from the model to develop design criteria for the future development of small molecule agents for targeted cancer therapeutics.

*Corresponding Author: K. Dane Wittrup, Ph.D., Massachusetts Institute of Technology, 400 Main Street, E19-551, Cambridge, MA 02139, wittrup@mit.edu, Phone: 617-258-5279, Fax: 617-253-1954.

Conflicts of Interest:
Kelly Davis Orcutt: None.
John Rhoden: None.
Benjamin Ruiz-Yi: None.
John V. Frangioni: None.
K. Dane Wittrup: None.

### Keywords

Affinity; radioimmunotherapy; tumor targeting; DOTA; mathematical model

## INTRODUCTION

Radiolabeled agents have been used as delivery vehicles of ionizing radiation to specific disease sites for over 50 years (1–6). Their systemic administration allows the treatment of widely disseminated disease, as opposed to external beam radiotherapy, which is used for the treatment of known disease sites. Therapeutic radiopharmaceuticals are designed to exhibit high specificity to the targeted disease site with low accumulation in normal tissues producing minimal radiation damage to normal cells.

A large number of molecules have been considered for targeted delivery of radioisotopes, including radiolabeled antibodies, antibody fragments, alterative scaffolds, and small molecules (7–10). While antibodies exhibit excellent binding specificity, they also exhibit long half-lives in the blood resulting in low tumor-to-background ratios. Antibody fragments and other smaller binding scaffolds exhibit faster blood clearance, but result in high kidney and/or liver uptake. Radiolabeled small molecule ligands generally exhibit more rapid blood clearance and lower background compared to antibodies and antibody fragments, but usually result in poor specificity due to relatively low affinities for the desired target. Thus, there is a strong interest in developing small molecules with higher affinities both through improved high-throughput screening techniques (11) and through affinity enhancement using avidity (12–14).

Another approach to generate high affinity binding of small molecules to disease sites is to use a method called pretargeted radioimmunotherapy (15–17). This approach couples the high binding specificity of antibodies with the rapid clearance of radiolabeled small molecules, resulting in high tumor uptake yet fast clearance from non-tumor tissue.

We have engineered a high-affinity antibody fragment with specificity for DOTA-metal chelates for pretargeted radioimmunotherapy applications (18). A particularly unique feature of the engineered scaffold is its ability to bind to different DOTA-chelates with a wide range of affinities. Here, we use it in a pretargeted approach to systematically analyze the effect of affinity on tumor uptake *in vivo*. We compare these results to a compartmental model that has been extended from previous work and use simple analytical relations to derive design criteria to guide engineering efforts in the development of small molecule radiotherapeutics. We present here a unique analysis of affinity in tumor targeting and discuss its implications in pretargeted radioimmunotherapy and small molecule targeting.

## MATERIALS AND METHODS

### Reagents

1,4,7,10-Tetraazacyclododecane-1,4,7,10-tetraacetic acid (DOTA), *S*-2-(R-Aminobenzyl)-1,4,7,10-tetraazacyclododecane tetraacetic acid (DOTA-Bn), and *S*-2-(4-Isothiocyanatobenzyl)-1,4,7,10-tetraazacyclododecane tetraacetic acid (DOTA-SCN) were

purchased from Macrocyclics (Dallas, TX). All other chemicals were purchased from Sigma-Aldrich (St. Louis, MO) or Thermo Fisher Scientific (Waltham, MA) unless specified otherwise.Sm3e/C825 bsAb was produced by transient HEK cell transfection and purified as described (19).

### Synthesis of Dextran-based Clearing Agent

5 mg (10 nmol) of 500 kDa amino dextran purchased from Invitrogen (Carlsbad, CA) with 136 moles of amine per mole dextran was reacted with 3.7 mg (5.3 μmol) DOTA-SCN in 1 mL dimethyl sulfoxide (DMSO) with 1.9 μL (13.6 μmol) triethylamine TEA overnight at room temperature with mild vortexing. The dextran reaction mixture was diluted with 14 mL 0.4 M sodium acetate pH 5.2 and 53 μmol yttrium nitrate was added. The mixture was incubated overnight at 37°C, dialyzed against water, and then dried down by vacuum centrifugation. The dried dextran compound was resuspended in phosphate buffered saline (PBS) and purified by size exclusion chromatography using a Superdex 75 10/300 GL column. Fractions containing the dextran compound were combined, dialyzed against water twice, dried by vacuum centrifugation, resuspended in saline and 0.2 μm filtered. The final dextran-DOTA-Y contained approximately 130 DOTA molecules as assessed by a TNBSA assay (Thermo Fisher Scientific, Rockford, IL).

### Radiolabeling

DOTA and DOTABn were dissolved at 0.5 mM in ammonium acetate pH 5.6. 1–2 mCi $^{177}LuCl_3$ (PerkinElmer, Waltham, MA) or $^{111}InCl_3$ (Cardinal Health, Dublin, OH) were added to the metal chelate and incubated for 1–2 h at 85–95°C. The radiolabeled compounds were purified by RP-HPLC (14, 20) with gamma detection on a 4.6 × 75 mm Symmetry C18 column using a linear gradient from 0% to 40% B over 15 minutes, at a flow rate of 1 mL/min, where A = 10 mM TEAA and B = methanol. The purified compounds were dried under vacuum, resuspended in saline, and filter-sterilized.

$^{111}$In-DOTA-dextran was prepared by synthesizing dextran-DOTA as described above, without loading with cold yttrium. Dextran-DOTA was incubated with 1–2 mCi $^{111}InCl_3$ for 1 h at 37°C followed by concentration and dilution with saline as described above.

### Animal models

All animal handling was performed in accordance with Beth Israel Deaconess Medical Center Institutional Animal Care and Use Committee guidelines. LS174T and C6 cells were obtained from ATCC and maintained under standard conditions. The cell lines were confirmed to be negative for mycoplasma and mouse pathogens by the Yale Virology Lab. Xenograft tumors were established in left and right flanks, respectively, of 5–6 week-old make NCRU-nu/nu mice (Taconic Farms, Hudson, NY) as described previously (19).

### Pretargeted protocol

An IgG-basedbispecific antibody (bsAb), Sm3e/C825, that binds to CEA and DOTA-metal chelates has been previously described (19). The bsAb binds to CEA with an apparent affinity of ~100 pM and to $^{177}$Lu-DOTABn, $^{177}$Lu-DOTA, $^{111}$In-DOTABn and $^{111}$In-DOTA with affinities of approximately 10 pM, 400 pM, 1 nM, and 20 nM, respectively (18,

19).500 ug (2.5 nmol)Sm3e/C825 bsAb (19) was intravenously injected into LS174T and C6 (CEA-negative tumor used as a controlfor nonspecific tumor uptake) tumor-bearing mice followed by intravenous injection of 250 ug (0.45 nmol) dextran clearing agent 24 h later to clear residual bsAb in the blood prior to administration of the radiolabeled DOTA.100–150 μCi (2–8 pmol) $^{177}$Lu-DOTABn, $^{177}$Lu-DOTA, $^{111}$In-DOTABn or $^{111}$In-DOTA was injected intravenously 1 h following clearing agent administration. Blood was collected from the tail vein using micro-capillary tubes and counted on a model 1470 Wallac Wizard (PerkinElmer, Wellesley, MA) 10-detector gamma counter. At various times, mice were euthanized by intraperitoneal injection of pentobarbital followed by cervical dislocation, a method consistent with the recommendations of the Panel on Euthanasia of the American Veterinary Medical Association. Organs and tumors were resected, washed three times in PBS, weighed, and counted as described above.

## Imaging

SPECT/CT (single photon emission computed tomography/computed tomography) scans and image analyses were performed using a rodent scanner (NanoSPECT/CT, Bioscan, Washington, DC) equipped with an 8W x-ray source running at 45 kV (177 μA), and a 48 μm pitch CMOS-CCD x-ray detector. Mice were anesthetized in an anesthetic chamber with isoflurane and transferred to a bed on a gantry for imaging where gas anesthesia was maintained for the duration of the scan. After acquisition of a CT topogram, helical micro SPECT was performed using a four-headed gamma camera outfitted with multi-pinhole collimators (1.4 mm) and a total scan time of 45 min. SPECT images were acquired over 360° in 24 projections each using a 256 × 256 frame size (1.0 mm pixels). Images were reconstructed with Bioscan HiSPECT iterative reconstruction software and fused with CT images. Immediately after scanning, mice were sacrificed; tissues and tumors were weighed and counted as described above.

## Mathematical Model

Tumor uptake of radiolabeled small molecules was simulated using a mechanistic compartmental model extended from previous work (21, 22), with the assumption that radioisotope that is internalized into cells remains trapped within the cell (Supplementary Materials and Methods). The tumor concentration of residualizing isotope following a sub-saturating intravenous injection of radiolabeled small molecule can therefore be described as:

$$C_{tumor}=\frac{K^{trans}C_{p0}}{\psi-k_{cl}}\left((e^{-k_{cl}t}-e^{-\psi t})+\frac{BP}{1+BP}k_e\left(\frac{1-e^{-k_{cl}t}}{k_{cl}}-\frac{1-e^{-\psi t}}{\psi}\right)\right) \quad (1)$$

$$\psi=\frac{\frac{K^{trans}}{\varepsilon}+k_eBP}{1+BP} \quad (2)$$

Where $C_{tumor}$ is the overall concentration of the isotope in the tumor, t is time, $C_{p0}$ is the initial plasma concentration of the radiolabeled small molecule, $k_e$ is the rate of endocytosis ($s^{-1}$), BP is the binding potential $B_{max}/K_D$,$B_{max}$ is the concentration of total antigen in the

tumor and $K_D$ is the binding affinity, $K^{trans}$ is the transcapillary transport rate ($s^{-1}$), $k_{cl}$ is the plasma clearance rate of the small molecule ($s^{-1}$), and $\varepsilon$ is the available volume fraction of the small molecule in the tumor. Parameter values were measured experimentally as described or obtained from published literature (Supplementary Table S1).

Using the above model, the concentration of residualized isotope in the tumor as time goes to infinity is:

$$C_{resid}=C_{p0}\frac{K^{trans}}{k_{cl}}\frac{BP}{BP+\frac{K^{trans}/\varepsilon}{k_e}} \quad (3)$$

## RESULTS

The bispecific antibody Sm3e/C825, composed of the engineered high-affinity antibody fragment C825 with specificity for DOTA-metal chelates (18), was used in a pretargeted protocol to target DOTA-chelates to CEA-expressing xenograft tumors. A schematic depicting the pretargeted approach is shown in Figure 1.C825 binds to different DOTA-chelates with widely varying affinities dependent on the chelated metal and the presence or lack of an aminobenzene group attached to a carbon in the macrocycle backbone of DOTA. The organ/tissue biodistribution at 24 h post-injection of the hapten($^{177}$Lu-DOTABn, $^{177}$Lu-DOTA, $^{111}$In-DOTABn or $^{111}$In-DOTA) was determined in tumor-bearing mice (Figure 2 and Supplementary Table S2). The activity in the LS174T tumor increased with increasing hapten affinity from 0.5 ± 0.1 %ID/g for $^{111}$In-DOTA ($K_D$ = 20 nM) to 1.6 ± 0.3 %ID/g for $^{111}$In-DOTABn ($K_D$ = 1 nM) to 14.3 ± 1.8 %ID/g for $^{177}$Lu-DOTA ($K_D$ = 400 pM). The tumor activity for $^{177}$Lu-DOTABn ($K_D$ = 10 pM) was 19 ± 4 %ID/g and not significantly different than that of the 400 pM affinity $^{177}$Lu-DOTA. The activity in the C6 antigen-negative tumor also increased with affinity, due to higher-affinity binding to bsAb retained nonspecifically through the enhanced permeability and retention (EPR) effect (23). Activities in non-tumor tissues are also higher for the highest affinity compounds due to higher affinity binding to residual bsAb. The tumor-to-kidney ratio increased from 1.2 ± 0.4 for ~20 nM to 17 ± 3 for ~400 pM, but then decreased to 10 ± 2 for ~10 pM affinity due to higher uptake in the kidney yet similar tumor uptake. Similarly, the tumor-to-blood ratio was highest for 400 pM affinity $^{177}$Lu-DOTA at 380 ± 90.

One mouse from each affinity group was imaged by SPECT/CT (Figure 3). For the $^{111}$In isotope, visible tumor signal is observed in the antigen-positive LS174T tumor at 24 h p.i. for 1 nM $^{111}$In-DOTABn, however, no significant signal is observed for 20 nM $^{111}$In-DOTA. For the $^{177}$Lu-isotope, excellent tumor targeting is observed for both 400 pM $^{177}$Lu-DOTA and 10 pM $^{177}$Lu-DOTABn. Some signal is also observed in the antigen-negative tumors, as expected from the biodistribution data. It should be noted that while $^{111}$In and $^{177}$Lu have similar reconstructed resolutions, the average sensitivity of $^{111}$In is about five times greater than $^{177}$Lu in mice (24).

The use of the clearing agent one hour prior to hapten administration resulted in significantly better tumor-to-background ratios compared to a two-step protocol

(Supplementary Figure S1). For the pretargeted protocol, the dextran-DOTA compound was loaded with non-radioactive yttrium as it is one of the metals, when chelated to DOTA and DOTA-Bn, that exhibits the highest affinity to C8.2.5. The clearingagent clears rapidly from the blood through the liver and spleen with no observable tumor accumulation (Supplementary Figure S2).

Because the $^{177}$Lu-DOTA compound resulted in the highest tumor-to-background ratios of the four DOTA haptens, it was further characterized for pretargeted radioimmunotherapy applications. At 4 h post-injection of $^{177}$Lu-DOTA, tumor uptake was 7.44 0.41 %ID/g in the antigen-positive tumor (Table 1 and Supplementary Figure S3), approximately 90-fold higher than the tumor uptake observed for $^{177}$Lu-DOTA alone (Table 1). Tumor uptake in the antigen-negative tumor was 9.82 0.35 %ID/g at 4 h, similar to the antigen-positive tumor due to the EPR effect. Over time, the tumor activity in the antigen-negative tumor decreased to 4.23 ± 0.54 %ID/g at 24 h and 2.89 ± 2.28 %ID/g at 48 h while the tumor activity in the antigen-positive tumor increased to 14.3 ± 1.8 %ID/g at 24 h and remained essentially constant at 48 h. The LS174T tumor-to-blood ratio increased from 18 ± 2 at 4 h to 380 ± 90 at 24 h and was greater than 450 at 48 h (Table 2). At 48 h, the blood activity was not measurable above background. The LS174T tumor-to-kidney ratio increased from approximately 8 at 4 h to about 20 at 24 and 48 h.

We developed a mathematical modelbased on an extension to a previously published compartmental model of tumor uptake of targeted agents (25). The model uses only measurable parameters, with no fit variables (Supplementary Table S1). The transcapillary transport rate of the DOTA-based compounds was assumed to be similar to that for Gd-DTPA (26).This model applies only to residualizing isotopes and targeted molecules that are not cell permeable. For radiotherapy, the goal is to retain the isotope for an extended period of time to allow for radioactive decay at the site of the tumor. It is known that radioactive metals and some forms of iodine are residualizing and retained intracellularly after internalization (27–29). Derivation of the model is provided in the Supplemental Materials and Methods. The analytical solution allows straightforward analysis of the effect of changing parameters on tumor uptake.

$$\lim_{t\to\infty} C_{resid} = \frac{K^{trans}}{k_{cl}} C_{po} \frac{BP}{BP + {K^{trans}}/{\varepsilon}\, k_e} \quad (4)$$

From this equation, we derive a metric for affinity, BP >$K^{trans}$/(ε*$k_e$), for maximum tumor uptake of isotope for a given radiotherapeutic/antigen system. From this metric, we predict that faster internalization will lead to a lower affinity requirement and that higher affinity is required for ligands with faster transcapillary transport and for antigen targets with lower $B_{max}$.

For the particular system studied here, $\frac{K^{trans}/\varepsilon}{k_e} \approx 400$, therefore it is predicted that saturating levels of signal should be obtained with $BP = \frac{B_{\max}}{K_d} > 400$. For our measured value

of, this $B_{max}$ = 200 nM, corresponds to $K_d$ < 0.5 nM, consistent with the experimental results (Figure 4). Equation 4 also predicts a maximal residualized tumor signal of $\lim_{t\to\infty} C_{resid} = \frac{K^{trans}}{k_{cl}} C_{po}$ for the highest affinity capture; thus for the parameters in this system, $\lim_{t\to\infty} C_{resid} = 0.3C_{po} \cong 15$ %ID/g is the predicted highest dose attainable.

The experimental results of tumor uptake versus affinity compared very well to model prediction (Figure 4) with the 24 h tumor uptake increasing significantly from single-digit nanomolar to picomolar affinity and then reaching a plateau.

## DISCUSSION

Here, we present a systematic study of the effect of affinity on tumor uptake of DOTA-metal haptens using a previously engineered bsAb that binds with varying affinities to different DOTA chelates (18). The effect of binding affinity on tumor uptake has been previously described for antibodies and antibody fragments (30, 31). However, this is the first time, to our knowledge, that the effect of binding affinity on tumor targeting of a small molecule has been studied *in vivo* with the same target antigen resulting in unaltered internalization kinetics and $B_{max}$. Four compounds spanning a range of affinities over three orders of magnitude were studied. We show here that an affinity of 400 pM is required for maximum uptake in the studied system with an internalization half-life of about 13 h and a $B_{max}$ on the order of 200 nM ($10^5$–$10^6$ binding sites/cell assuming typical cell densities for a vascular xenograft tumor (32)). Further improvement in affinity to 10 pM affinity does not significantly improve tumor uptake.

Tumor uptake of radiolabeled small molecules was simulated using a mechanistic compartmental model extended from previous work. The experimental results were consistent with model simulations. We further derived analytical relations to provide design criteria to guide engineering efforts in the development of small molecule radiotherapeutics. The design criteria allow for prediction of a target affinity for the development of new radiotherapeutic agents. These relationships can guide experimental efforts in drug development.

The experimental and mathematical model results presented here suggest that a plateau exists for any given ligand/receptor pair such that further improvements in affinity result in no additional improvement in tumor uptake. The affinity range at which this plateau exists depends on the $B_{max}$, $k_e$, $K^{trans}$, and ε of the particular ligand and antigen. For example, in the system studied here, if $B_{max}$were reduced from 200 nM to 20 nM, saturating levels of signal would require a 10-fold improvement in affinity. Beyond a given affinity, additional affinity improvement may result in decreased therapeutic efficacy in some applications by resulting in higher background due to improved binding to residual bsAb present at low concentrations in PRIT applications or improved uptake in normal tissues with low levels of antigen expression in one-step approaches.

It should be noted that the clearing agent did not appear to completely clear circulating bsAb, as the amount of background signal increased with increasing hapten affinity (Figure

2). In addition, the LS174T tumor activity increases from 4 to 24 hours for pretargeted $^{177}$Lu-DOTA (Supplementary Figure S3). While the simplified model presented here does not take antibody kinetics into account, the correlation of the experimental data with the model suggest the relationships derived here may be useful in the design of tumor-targeting small molecules. Additional experiments with more efficient clearing of the bsAb would provide further data to support the model.

In addition to the affinity series, we present a method for pretargeted radioimmunotherapy that uses an IgG-scFv bsAb, a dextran-based clearing agent, and radiolabeled DOTA. $^{177}$Lu-DOTA has previously been shown to exhibit very rapid whole-body clearance from mice (33). Here we demonstrate high LS174T tumor uptake and retention of $^{177}$Lu-DOTA with fast clearance from non-tumor tissue resulting in the highest yet reported tumor-to-kidney ratios at 48 h p.i. for CEA targeting.

A significant amount of $^{177}$Lu-DOTA uptake is observed in the CEA-negative tumors at early times. The EPR effect results in nonspecific tumor accumulation of high-molecular weight compounds. While approximately 4-fold higher bsAb uptake is observed in LS174T tumors versus C6 tumors (19), a significant fraction of the bsAb localized to the LS174T tumors will be inaccessible to binding due to the ~13 h internalization half-life of CEA (34), while all bsAb in the C6 tumors will be accessible to hapten binding. This is consistent with the observation of similarhapten activities in the two tumors at early times. At later times, unbound antibody slowly intravasates out of the CEA-negative tumor while CEA-bound antibody in the LS174T tumors internalizes $^{177}$Lu-DOTA compounds where the radiolabel is trapped within the cell.

An engineered IgG-like bsAb was used here to harness the established therapeutic advantages of IgGs. The bsAb possesses slow blood clearance resulting in high tumor uptake, retains potentially beneficial secondary immune function, and can be produced and purified in a fashion identical to that of an IgG (19). The system uses DOTA-chelated metal as the hapten, with no additional synthesis or modification required. This eliminates any issues with linker cleavage and peptide stability that have been reported for other haptens in PRIT applications (35, 36).DOTA chelated to gadolinium has been administered to human subjects in millimolar concentrations and has an established safety profile. DOTA-metal chelates exhibit rapid blood clearance and whole-body clearance observed in mice (33)and humans (37). A particularly useful advantage to the approach described here is that only radiolabeled DOTA will bind to the pretargeted anti-DOTA binding sites, while unlabeled DOTA exhibits no observable binding. This results in very high effective specific activity without requiring complex and time-consuming purification schemes.

While three-step pretargeted radioimmunotherapy adds complexity over two-step procedures, it allows higher doses of bsAb to be administered resulting in higher achieved tumor doses as well as more homogenous distribution within the tumor (38). In addition, it allows for possible secondary immune effects resulting from the retained Fc domain that may prove significant (39). Two-step approaches may be sufficient for molecular imaging leading to improved cancer screening and staging(40, 41). However, it is anticipated that the

increased number of hapten binding sites afforded by three-step approaches will prove critical for therapy.

We present here a method for pretargeted radioimmunotherapy and use it in a systematic study of the effect of small molecule affinity on tumor uptake *in vivo* with affinities spanning a range of three orders of magnitude. In addition, we develop a mathematical model of tumor targeting using only known, measured parameters that correlates well with experimental observations. We predict that this model will be useful for rational design of new agents and to guide experimental efforts in the development and optimization of targeted cancer therapeutics.

## Supplementary Material

Refer to Web version on PubMed Central for supplementary material.

## Acknowledgments

The authors acknowledge David G. Whitehead and Fangbing Liu, Ph.D. for help with cell culture, Elaine P. Lunsford for assistance with SPECT/CT imaging, HakSoo Choi, Ph.D. for helpful discussions, Lorissa Moffitt for editing, and Eugenia Trabucchi and Donald McGaffigan for administrative support.

**GRANT SUPPORT**

National Science Foundation Graduate Research Fellowships (KDO, JR)

Lewis Family Fund (JVF)

National Institutes of Health grant R01-CA-101830 (KDW)

## Abbreviations

| | |
|---|---|
| **DOTA** | 1,4,7,10-Tetraazacyclododecane-1,4,7,10-tetraacetic acid |
| **DOTA-Bn** | *S*-2-(RAminobenzyl)-1,4,7,10-tetraazacyclododecane tetraacetic acid |
| **DMSO** | dimethyl sulfoxide |
| **TEA** | triethylamine |
| **PBS** | phosphate buffered saline |
| **SPECT** | single photon emission computed tomography |
| **CT** | computed tomography |
| **CEA** | carcinoembryonic antigen |

## References

1. Beierwaltes WH. Radioiodine therapy of thyroid disease. Int J Rad Appl Instrum B. 1987; 14:177–181. [PubMed: 3312117]
2. Britton KE. Towards the goal of cancer-specific imaging and therapy. Nucl Med Commun. 1997; 18:992–1007. [PubMed: 9423199]
3. Firusian N, Mellin P, Schmidt CG. Results of 89strontium therapy in patients with carcinoma of the prostate and incurable pain from bone metastases: a preliminary report. J Urol. 1976; 116:764–768. [PubMed: 1003647]

4. Hoefnagel CA. Anti-cancer radiopharmaceuticals. Anticancer Drugs. 1991; 2:107–132. [PubMed: 1958857]
5. Larson SM. Radioimmunology. Imaging and therapy. Cancer. 1991; 67:1253–1260. [PubMed: 1991286]
6. Winston MA. Radioisotope therapy in bone and joint disease. Semin Nucl Med. 1979; 9:114–120. [PubMed: 90387]
7. Wiseman GA, White CA, Witzig TE, Gordon LI, Emmanouilides C, Raubitschek A, et al. Radioimmunotherapy of relapsed non-Hodgkin's lymphoma with zevalin, a 90Y-labeled anti-CD20 monoclonal antibody. Clin Cancer Res. 1999; 5:3281s–3286s. [PubMed: 10541376]
8. Tolmachev V, Orlova A, Pehrson R, Galli J, Baastrup B, Andersson K, et al. Radionuclide therapy of HER2-positive microxenografts using a 177Lu-labeled HER2-specific Affibody molecule. Cancer Res. 2007; 67:2773–2782. [PubMed: 17363599]
9. Birchler MT, Thuerl C, Schmid D, Neri D, Waibel R, Schubiger A, et al. Immunoscintigraphy of patients with head and neck carcinomas, with an anti-angiogenetic antibody fragment. Otolaryngol Head Neck Surg. 2007; 136:543–548. [PubMed: 17418248]
10. Reubi JC, Maecke HR. Peptide-based probes for cancer imaging. J Nucl Med. 2008; 49:1735–1738. [PubMed: 18927341]
11. Peng L, Liu R, Marik J, Wang X, Takada Y, Lam KS. Combinatorial chemistry identifies high-affinity peptidomimetics against alpha4beta1 integrin for in vivo tumor imaging. Nat Chem Biol. 2006; 2:381–389. [PubMed: 16767086]
12. Mammen M, Choi S, Whitesides GM. Polyvalent interactions in biological systems: Implications for design and use of multivalent ligands and inhibitors. Angewandte Chemie International Edition. 1998; 37:2754–2794.
13. Humblet V, Misra P, Bhushan KR, Nasr K, Ko YS, Tsukamoto T, et al. Multivalent scaffolds for affinity maturation of small molecule cell surface binders and their application to prostate tumor targeting. J Med Chem. 2009; 52:544–550. [PubMed: 19108655]
14. Misra P, Humblet V, Pannier N, Maison W, Frangioni JV. Production of multimeric prostate-specific membrane antigen small-molecule radiotracers using a solid-phase 99mTc preloading strategy. J Nucl Med. 2007; 48:1379–1389. [PubMed: 17631555]
15. Goodwin DA, Meares CF, McCall MJ, McTigue M, Chaovapong W. Pre-targeted immunoscintigraphy of murine tumors with indium-111-labeled bifunctional haptens. J Nucl Med. 1988; 29:226–234. [PubMed: 3346734]
16. Sharkey RM, Karacay H, Cardillo TM, Chang CH, McBride WJ, Rossi EA, et al. Improving the delivery of radionuclides for imaging and therapy of cancer using pretargeting methods. Clin Cancer Res. 2005; 11:7109s–7121s. [PubMed: 16203810]
17. Boerman OC, van Schaijk FG, Oyen WJ, Corstens FH. Pretargeted radioimmunotherapy of cancer: progress step by step. J Nucl Med. 2003; 44:400–411. [PubMed: 12621007]
18. Orcutt KD, Slusarczyk AL, Cieslewicz M, Ruiz-Yi B, Bhushan KR, Frangioni JV, et al. Engineering an antibody with picomolar affinity to DOTA chelates of multiple radionuclides for pretargeted radioimmunotherapy and imaging. Nucl Med Biol. 2011; 38:223–233. [PubMed: 21315278]
19. Orcutt KD, Ackerman ME, Cieslewicz M, Quiroz E, Slusarczyk AL, Frangioni JV, et al. A modular IgG-scFv bispecific antibody topology. Protein Eng Des Sel. 2010; 23:221–228. [PubMed: 20019028]
20. Humblet V, Misra P, Frangioni JV. An HPLC/mass spectrometry platform for the development of multimodality contrast agents and targeted therapeutics: prostate-specific membrane antigen small molecule derivatives. Contrast Media Mol Imaging. 2006; 1:196–211. [PubMed: 17193697]
21. Schmidt MM, Wittrup KD. A modeling analysis of the effects of molecular size and binding affinity on tumor targeting. Mol Cancer Ther. 2009; 8:2861–2871. [PubMed: 19825804]
22. Tofts PS, Brix G, Buckley DL, Evelhoch JL, Henderson E, Knopp MV, et al. Estimating kinetic parameters from dynamic contrast-enhanced T(1)-weighted MRI of a diffusable tracer: standardized quantities and symbols. J Magn Reson Imaging. 1999; 10:223–232. [PubMed: 10508281]

23. Maeda H, Wu J, Sawa T, Matsumura Y, Hori K. Tumor vascular permeability and the EPR effect in macromolecular therapeutics: a review. J Control Release. 2000; 65:271–284. [PubMed: 10699287]
24. Hoppin J, Orcutt KD, Hesterman JY, Silva MD, Cheng D, Lackas C, et al. Assessing antibody pharmacokinetics in mice with in vivo imaging. J Pharmacol Exp Ther. 337:350–358. [PubMed: 21317355]
25. Schmidt MM, Wittrup KD. A modeling analysis of the effects of molecular size and binding affinity on tumor targeting. Mol Cancer Ther. 2009; 8:2861–2871. [PubMed: 19825804]
26. Daldrup H, Shames DM, Wendland M, Okuhata Y, Link TM, Rosenau W, et al. Correlation of dynamic contrast-enhanced MR imaging with histologic tumor grade: comparison of macromolecular and small-molecular contrast media. AJR Am J Roentgenol. 1998; 171:941–949. [PubMed: 9762973]
27. Shih LB, Thorpe SR, Griffiths GL, Diril H, Ong GL, Hansen HJ, et al. The processing and fate of antibodies and their radiolabels bound to the surface of tumor cells in vitro: a comparison of nine radiolabels. J Nucl Med. 1994; 35:899–908. [PubMed: 8176479]
28. Stein R, Govindan SV, Mattes MJ, Chen S, Reed L, Newsome G, et al. Improved iodine radiolabels for monoclonal antibody therapy. Cancer Res. 2003; 63:111–118. [PubMed: 12517786]
29. Press OW, Shan D, Howell-Clark J, Eary J, Appelbaum FR, Matthews D, et al. Comparative metabolism and retention of iodine-125, yttrium-90, and indium-111 radioimmunoconjugates by cancer cells. Cancer Res. 1996; 56:2123–2129. [PubMed: 8616860]
30. Adams GP, Schier R, McCall AM, Simmons HH, Horak EM, Alpaugh RK, et al. High affinity restricts the localization and tumor penetration of single-chain fv antibody molecules. Cancer Res. 2001; 61:4750–4755. [PubMed: 11406547]
31. Rudnick SI, Lou J, Shaller CC, Tang Y, Klein-Szanto AJ, Weiner LM, et al. Influence of affinity and antigen internalization on the uptake and penetration of Anti-HER2 antibodies in solid tumors. Cancer Res. 71:2250–2259. [PubMed: 21406401]
32. Thurber GM, Zajic SC, Wittrup KD. Theoretic criteria for antibody penetration into solid tumors and micrometastases. J Nucl Med. 2007; 48:995–999. [PubMed: 17504872]
33. Orcutt KD, Nasr K, Whitehead DG, Frangioni JV, Wittrup KD. Biodistribution and clearance of small molecule hapten chelates for pretargeted radioimmunotherapy. Mol Imaging Biol. 2011; 13:215–221. [PubMed: 20533093]
34. Schmidt MM, Thurber GM, Wittrup KD. Kinetics of anti-carcinoembryonic antigen antibody internalization: effects of affinity, bivalency, and stability. Cancer Immunol Immunother. 2008
35. van Gog FB, Visser GW, Gowrising RW, Snow GB, van Dongen GA. Synthesis and evaluation of 99mTc/99Tc-MAG3-biotin conjugates for antibody pretargeting strategies. Nucl Med Biol. 1998; 25:611–619. [PubMed: 9804042]
36. van Schaijk FG, Oosterwijk E, Soede AC, Broekema M, Frielink C, McBride WJ, et al. Pretargeting of carcinoembryonic antigen-expressing tumors with a biologically produced bispecific anticarcinoembryonic antigen × anti-indium-labeled diethylenetriaminepentaacetic acid antibody. Clin Cancer Res. 2005; 11:7130s–7136s. [PubMed: 16203812]
37. Le Mignon MM, Chambon C, Warrington S, Davies R, Bonnemain B. Gd-DOTA. Pharmacokinetics and tolerability after intravenous injection into healthy volunteers. Invest Radiol. 1990; 25:933–937. [PubMed: 2394577]
38. Blumenthal RD, Fand I, Sharkey RM, Boerman OC, Kashi R, Goldenberg DM. The effect of antibody protein dose on the uniformity of tumor distribution of radioantibodies: an autoradiographic study. Cancer Immunol Immunother. 1991; 33:351–358. [PubMed: 1652355]
39. Sharkey RM, Karacay H, Johnson CR, Litwin S, Rossi EA, McBride WJ, et al. Pretargeted versus directly targeted radioimmunotherapy combined with anti-CD20 antibody consolidation therapy of non-Hodgkin lymphoma. J Nucl Med. 2009; 50:444–453. [PubMed: 19223402]
40. Sharkey RM, Cardillo TM, Rossi EA, Chang CH, Karacay H, McBride WJ, et al. Signal amplification in molecular imaging by pretargeting a multivalent, bispecific antibody. Nat Med. 2005; 11:1250–1255. [PubMed: 16258537]

41. Sharkey RM, Karacay H, Vallabhajosula S, McBride WJ, Rossi EA, Chang CH, et al. Metastatic human colonic carcinoma: molecular imaging with pretargeted SPECT and PET in a mouse model. Radiology. 2008; 246:497–507. [PubMed: 18227543]

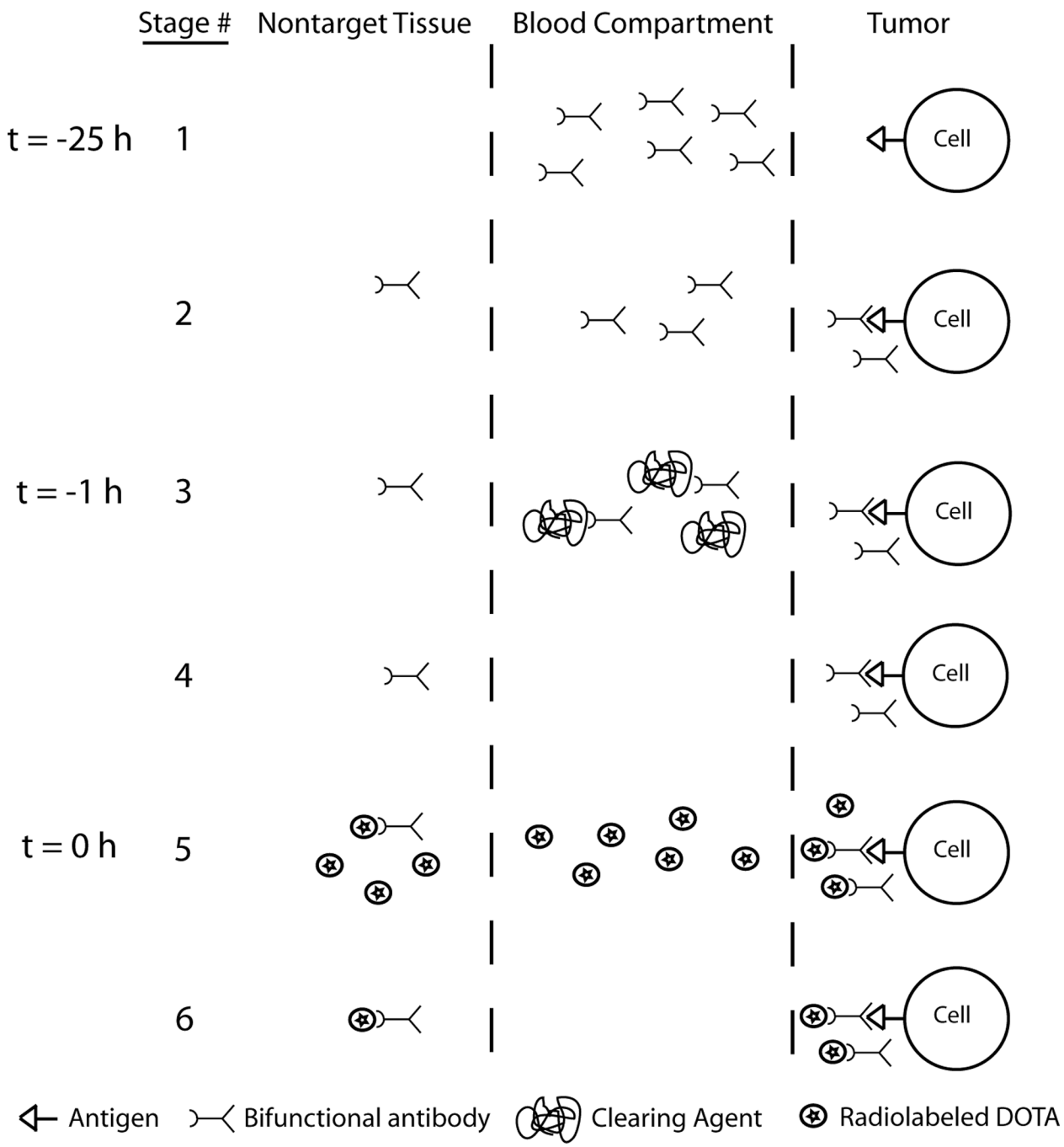


**Figure 1.**

Schematic of Pretargeted Radioimmunotherapy. A bifunctional antibody is administered in stage 1 and allowed to localize to tumor tissue in stage 2. In stage 3, a dextran clearing agent is administered. The clearing agent binds to bifunctional antibody in the blood compartment and clears it quickly as depicted in stage 4. Radiolabeled DOTA is administered in stage 5, where it binds to bifunctional antibody *in vivo* and clears rapidly via the kidneys in stage 6.

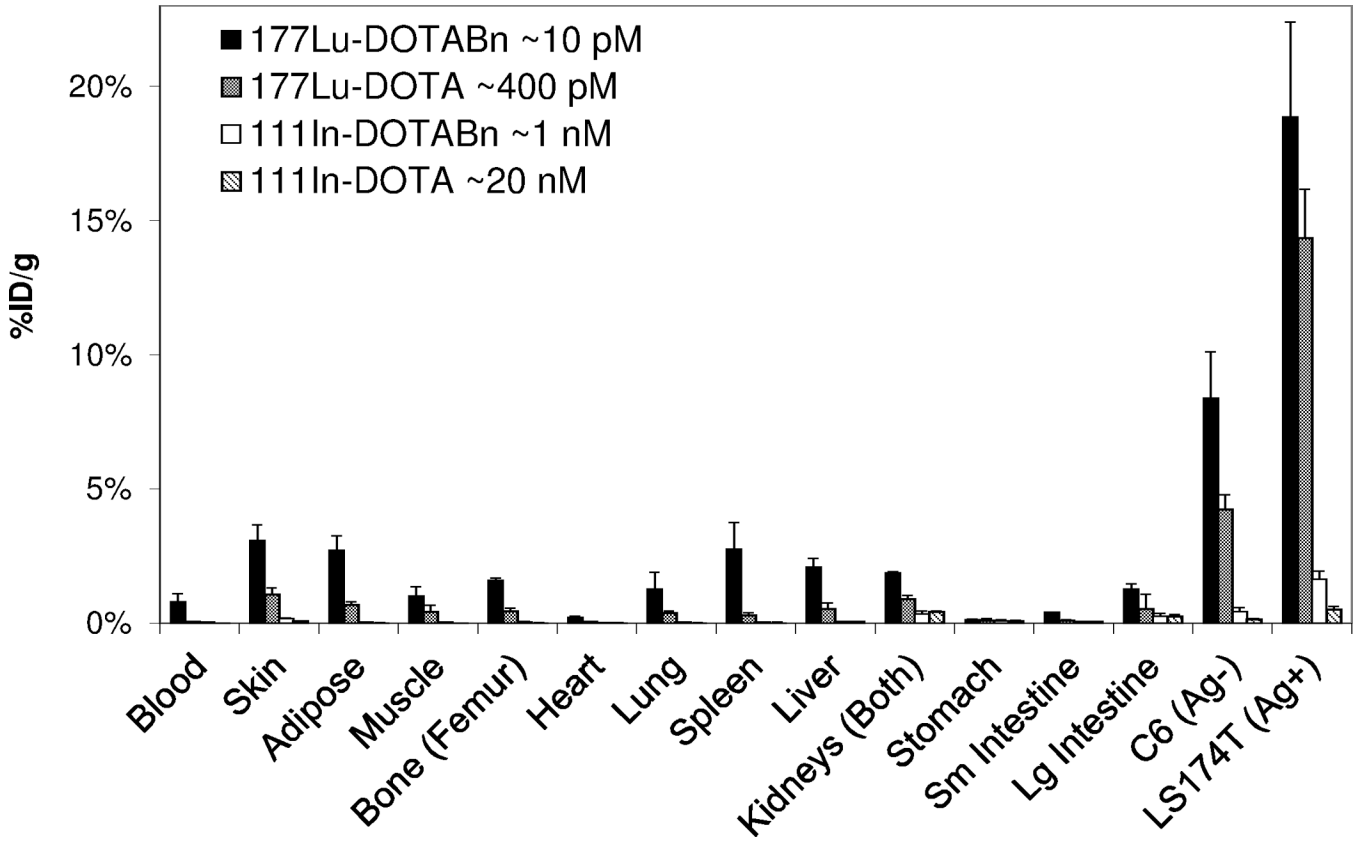


**Figure 2.**

Biodistribution of DOTA compounds with varying affinities. Organ/tissue biodistribution 24 h p.i. (mean ± S.D., n=3) of $^{177}$Lu-DOTA-Bn, $^{177}$Lu-DOTA, $^{111}$In-DOTA-Bn, and $^{111}$In-DOTA. 500 ug Sm3e/C825 bsAb was injected intravenously followed by 250 ug Y-DOTA-dextran clearing agent 24 h later. Radiolabeled DOTA was injected 1 h after the clearing agent.

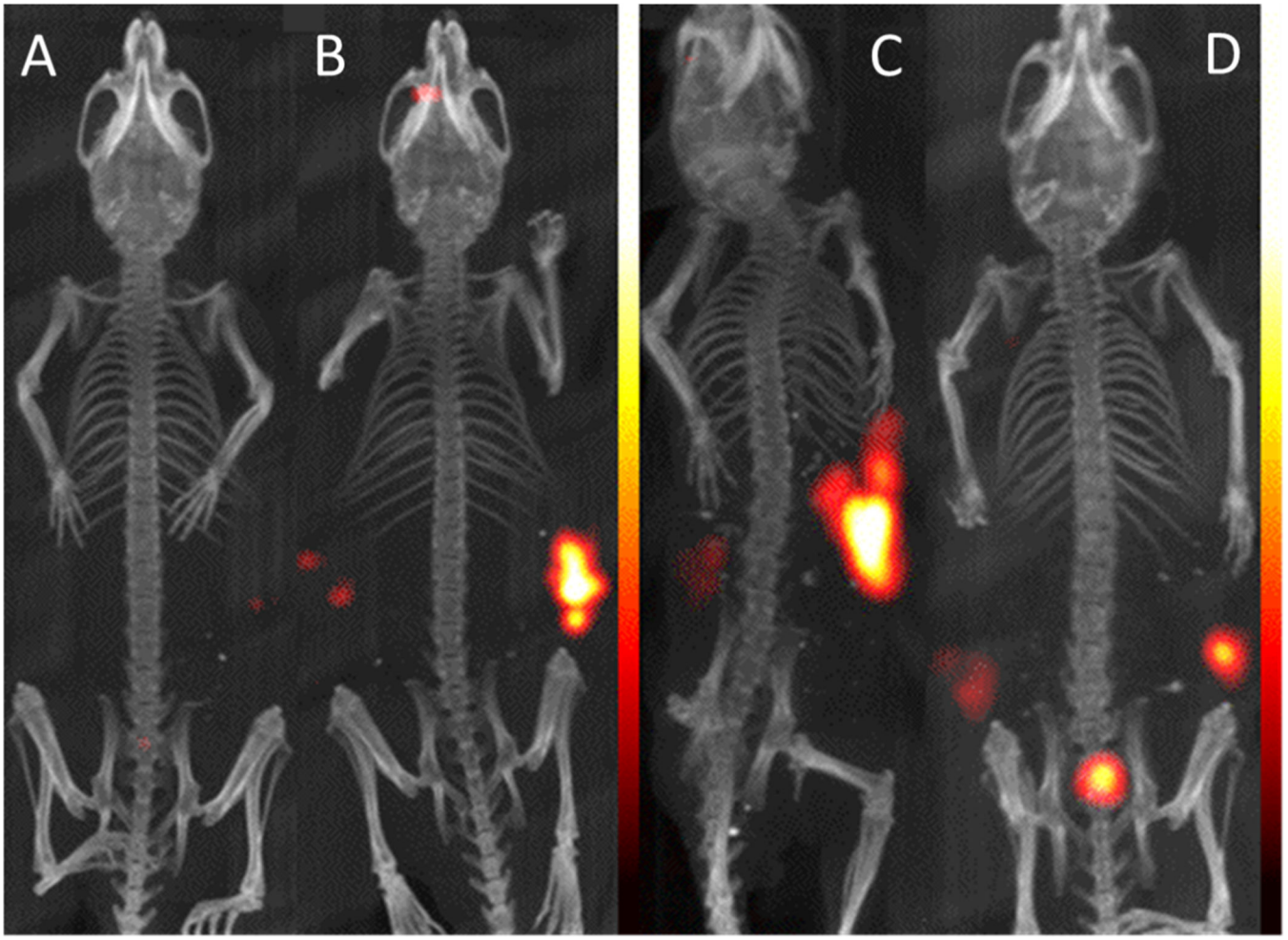


**Figure 3.**

SPECT/CT images of pretargeted DOTA compounds with varying affinities. SPECT/CT maximum intensity projections of tumor mice pretargeted with $^{111}$In-DOTA (A), $^{111}$In-DOTA-Bn (B), $^{177}$Lu-DOTA (C), and 177Lu-DOTA-Bn (D) 24 h p.i. Note that visualization of activity in the tumor(s) depends on both tumor activity and tumor size. Tumors were 0.1–0.4 g in size. Activity is observed in the bladder of some mice due to renal excretion.

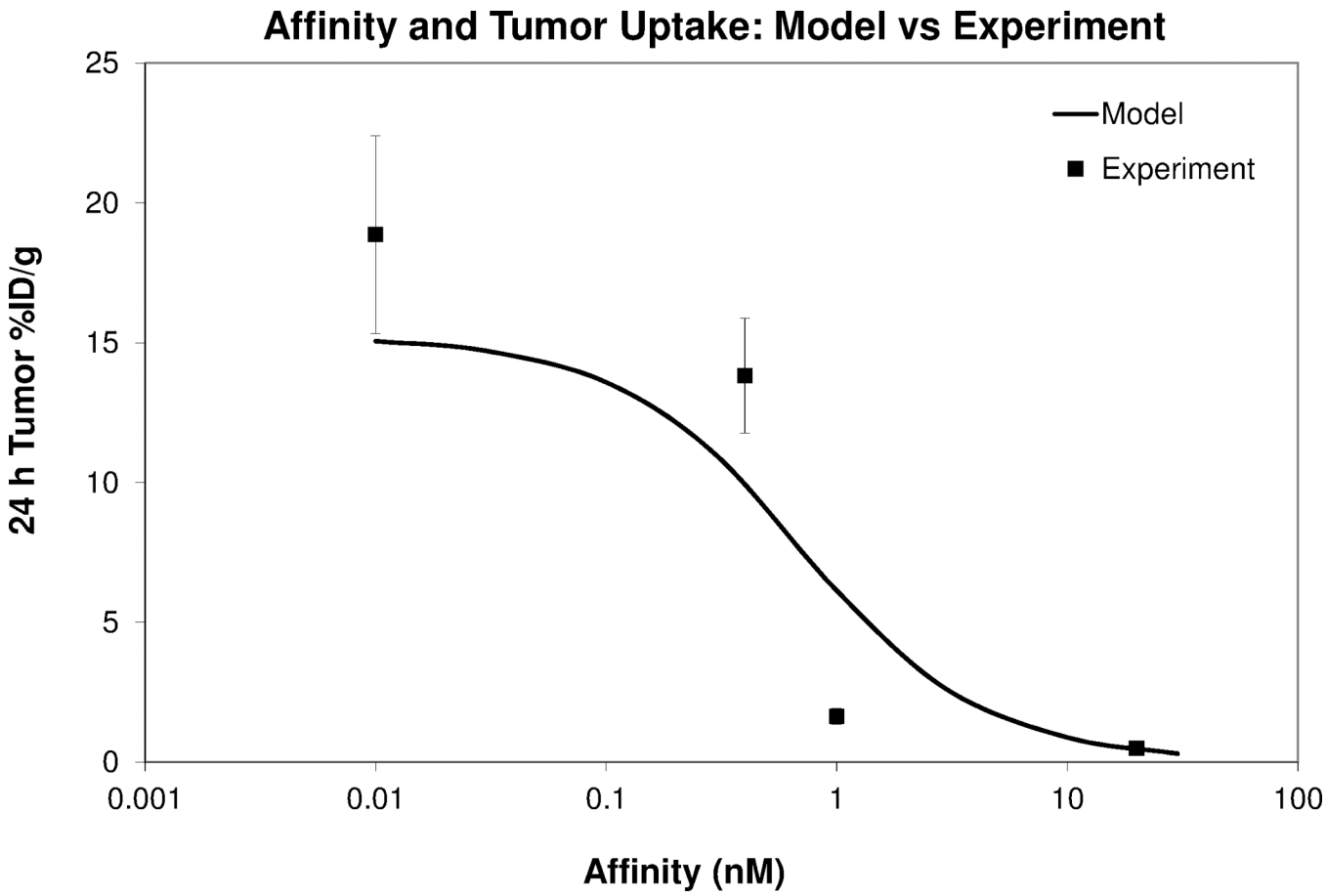


**Figure 4.**

24 h tumor uptake for varying affinities: mathematical prediction versus experimental results. Mathematical prediction (line) and experimental data (squares, mean ± s.d., n=3) of 24 h tumor %ID/g for increasing affinity. Model parameters: $t_{1/2,ke}$ = 13 h, $B_{max}$ = 226 nM, ε= 0.44, $t_{1/2,cl}$ = 2.07 min, $K^{trans}$ = 0.0022 $s^{-1}$.

## Table 1

Biodistribution of pretargeted $^{177}$Lu-DOTA

| | Time post-injection[a] | | |
|---|---|---|---|
| Organ/Tissue | 4 h | 24 h | 48 h |
| Blood | 0.42 ± 0.02 | 0.04 ± 0.01 | < 0.03 |
| Skin | 4.68 ± 1.06 | 1.05 ± 0.25 | 0.71 ± 0.20 |
| Adipose | 2.78 ± 1.08 | 0.67 ± 0.12 | 0.60 ± 0.29 |
| Muscle | 1.56 ± 0.56 | 0.41 ± 0.24 | 0.15 ± 0.07 |
| Bone (femur) | 1.49 ± 0.38 | 0.43 ± 0.12 | 0.24 ± 0.10 |
| Heart | 0.25 ± 0.16 | 0.05 ± 0.01 | 0.07 ± 0.03 |
| Lung | 1.25 ± 0.43 | 0.37 ± 0.07 | 0.21 ± 0.04 |
| Spleen | 0.39 ± 0.09 | 0.29 ± 0.09 | 0.64 ± 0.60 |
| Liver | 0.59 ± 0.21 | 0.51 ± 0.23 | 0.56 ± 0.35 |
| Kidneys (both) | 0.92 ± 0.05 | 0.88 ± 0.16 | 0.62 ± 0.19 |
| Stomach (with contents) | 0.21 ± 0.12 | 0.09 ± 0.07 | 0.22 ± 0.24 |
| Sm Intestine | 0.28 ± 0.02 | 0.08 ± 0.04 | 0.14 ± 0.11 |
| Lg Intestine | 0.13 ± 0.09 | 0.52 ± 0.56 | 0.11 ± 0.04 |
| C6 Tumor | 9.82 ± 0.35 (0.26 ± 0.08 g) | 4.23 ± 0.54 (0.26 ± 0.07 g) | 2.89 ± 2.28 (0.28 ± 0.13 g) |
| LS174T Tumor | 7.44 ± 0.41 (0.09 ± 0.03 g) | 14.34 ± 1.83 (0.21 ± 0.10 g) | 13.44 ± 3.25 (0.49 ± 0.09 g) |

[a]Mice were injected with 500 ug bsAb i.v. 24 h later, mice received 250 ug dextran-DOTA i.v. 1 h later, mice received 100–150 uCi of $^{177}$Lu-DOTA i.v. and were sacrificed at 4, 24, and 48 h p.i. Data given as mean ± s.d. (%ID/g, n=3). Tumor weights are provided as mean ± s.d. in parentheses.

## Table 2

Pretargeted tumor/organ ratios.

| | Time post-injection[a] | | |
|---|---|---|---|
| **Organ/tissue** | **4 h** | **24 h** | **48 h** |
| Blood | 18 ± 2 | 380 ± 90 | > 450 |
| Skin | 1.7 ± 0.4 | 14 ± 2 | 20 ± 8 |
| Adipose | 3.2 ± 1.5 | 23 ± 6 | 28 ± 13 |
| Muscle | 5.3 ± 1.6 | 57 ± 41 | 105 ± 40 |
| Bone (femur) | 5.3 ± 1.6 | 38 ± 16 | 60 ± 19 |
| Heart | 49 ± 36 | 323 ± 108 | 244 ± 85 |
| Lung | 7.2 ± 3.7 | 39 ± 3 | 63 ± 6 |
| Spleen | 20 ± 5 | 52 ± 12 | 40 ± 21 |
| Liver | 13.9 ± 3.7 | 33 ± 11 | 32 ± 13 |
| Kidneys (both) | 8.1 ± 0.2 | 17 ± 3 | 22 ± 3 |
| Stomach (with contents) | 48 ± 22 | 252 ± 119 | 276 ± 236 |
| Sm Intestine | 27 ± 4 | 217 ± 76 | 183 ± 129 |
| Lg Intestine | 80 ± 36 | 83 ± 53 | 128 ± 16 |
| C6 Tumor | 0.7 ± 0.1 | 3.4 ± 0.3 | 10 ± 9 |
| LS174T Tumor | 1 | 1 | 1 |

[a]Tumor/organ ratios (mean ± s.d., n=3) [a] Mice were injected with 500 ug bsAb i.v. 24 h later, mice received 250 ug dextran-DOTA i.v. 1 h later, mice received 100–150 uCi of $^{177}$ Lu-DOTA i.v. and were sacrificed at 4, 24, and 48 h p.i.